Journal of Energy Storage 45 (2022) 103696

Contents lists available at ScienceDirect

Journal of Energy Storage

journal homepage: www.elsevier.com/locate/est

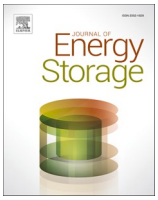

Research Papers

Numerical investigations of thermal performance enhancement in phase change energy storage system effective for solar adsorption cooling systems

V. Krishna Raj [a,b,*], V. Baiju [a], Faras P. Junaid [a]

[a] Energy Research Lab, Department of Mechanical Engineering, TKM College of Engineering, Kollam, Kerala, India
[b] A P J Abdul Kalam Technological University, Kerala, India

ARTICLE INFO

Keywords:
PCES
Preference selection index
Tapered fin
Solar adsorption chiller
Numerical studies
Phase change materials

ABSTRACT

Solar cooling systems requires an uninterrupted heat input for their continued operation. Thermal energy storage systems using phase change material (PCM) has the ability to deliver heat near isothermally and are effective for solar cooling applications. But these high energy dense storage systems exhibits poor thermal performance due to the low thermal conductivity of PCMs and are bulky. The main objective of this study is to design a phase change energy storage system (PCES) unit with different fin configurations, and to select a proper PCM for solar adsorption cooling systems (SAC). It projects the Preference Selection Index (PSI) method as the effective way to select the PCMs, and the result suggests the commercial PCM SavE-HS89 as a potential candidate among the different materials considered. This study also numerically investigates the thermal performance of different fins shapes, namely, positively tapered, negatively tapered and straight fins; among these the negatively tapered fins are found to be capable of compensating the slow melting process at the bottom region of the storage unit. It has been found that the negatively tapered fin improves the thermal performance of the PCES unit by reducing the melting time by up to 13% and 36% in comparison with the conventional straight fin and positively tapered fin, respectively. A case study of actual plant data of a SAC with different fin shapes shows that the storage system with the desirable configuration can save up to 46% of heat storage cost as compared to PCES without fin.

1. Introduction

In several countries like India, the share of space cooling in peak electricity load is expected to grow significantly, from 10% to 45% by the year 2050 [1]. To suppress this surge, researchers are emphasizing sustainable cooling methods, such as solar absorption and adsorption systems. Though the sorption cooling systems have lower coefficient of performance (COP) values as compared to the conventional vapour compression systems [2], their ability to use renewable energy and zero ozone depletion potential (ODP) got attention in the last few decades. Compared to absorption cooling devices, adsorption chillers' ability to operate at low heat source and less corrosion issues made them favourable [3].

The solar energy received is intermittent in nature, and hence the adsorption coolers generally require a thermal energy storage system (TES) to bridge the gap between the demand and supply of energy. Phase Change Energy Storage (PCES) system is the most promising one among various TESs, because of its high energy density.

The heat source temperature of different working pairs used in solar adsorption cooling system ranges from 60 °C-150 °C [4]. The most commonly used working pairs such as activated carbon – methanol, ethanol, R134a, R507a, CO_2, Silica gel – water, $CaCl_2$- $BaCl_2$ _ ammonia and hybrid activated carbon/silica gel working pairs requires heat input at a temperature of 80 °C for the desorption [5,6]. In recent years, a variety of theoretical and experimental studies of the use of TES unit in the Solar Adsorption Cooling Systems (SAC) has been reported. Abdellah El Fadar et.al [7] developed a mathematical model of SAC integrated with two types of TES units such as sensible and latent heat storage. The results show that the use of a latent heat storage unit (LHS) improves the solar COP and daily cooling production of the system by 48.24% and 48.27%, respectively. A similar study was conducted by Haghighi Poshtiri et.al [8] to find the efficiency of the solar cooling system integrated with an LHS unit. An auxiliary heater was also employed in addition to the main LHS unit. The study compared the performance of a SAC with and without an LHS unit. The study concludes that the application of LHS decreases auxiliary heat energy consumption by 7.32% and also increases the solar fraction by 8.82%. The feasibility of incorporating LHS units with solar cooling systems is already proven but they are still in the infant stage. Several studies also explore the methods

* Corresponding author.
E-mail addresses: krishnarajvvv@yahoo.com (V.K. Raj), baiju@tkmce.ac.in (V. Baiju).

https://doi.org/10.1016/j.est.2021.103696
Received 22 June 2021; Received in revised form 21 October 2021; Accepted 24 November 2021
Available online 6 December 2021
2352-152X/

Nomenclature

Abbreviations

AHP	analytical hierarchy process
CFD	computational fluid dynamics
COP	coefficient of performance
HTF	heat transfer fluid
MCDM	multi-criteria decision making
PCES	phase change energy storage system
PCM	phase change materials
PSI	preference selection index
SAS	solar adsorption systems
TOPSIS	techniques for order preference by similarity to ideal solution
TES	thermal energy storage

Symbols

A_{mushy}	mushy constant ($kg \bullet m^{-3} \bullet s^{-1}$)
Cp	specific heat ($kJ \bullet kg^{-1} \bullet k^{-1}$)
R	radius (m)
H	enthalpy ($kJ \bullet kg^{-1}$)
k	thermal conductivity ($W \bullet m^{-1} \bullet k^{-1}$)
H_f	enthalpy of fusion ($kJ \bullet kg^{-1}$)
M	mass (kg)
T	temperature (k)
C	cost (€)
f	liquid fraction
Re	Reynolds number

Greek symbols

β	thermal expansion coefficient (k−1)
μ	dynamic viscosity (kg•m−1•s−1)
Ø	fin parameter
ρ	density (kg•m−3)
t	time (s)

Subscripts

in	inlet
l	liquid-phase
max	maximum operating temperature
m	mean
s	solid-phase

to improve the performance of solar collectors and heat transfer fluids by using the nanofluid [9] and twisted tape inserts [10]. The type of phase change materials used inside the LHS has a major impact on its overall performance. So a systematic and comprehensive study is needed to select and rank the various PCMs suitable for solar adsorption cooling systems. PCMs have different thermophysical properties and costs. Multi-attribute decision making (MADM), an appropriate mathematical tool for the selection process and is the most widely employed for material selection based on its attributes or qualities. Analytical Hierarchy Process (AHP), Technique for Order Performance by Similarity to the Ideal Solution (TOPSIS), multi-criteria optimization and compromise solution (VIKOR) are the popular MCDM methods used. Ming-Chyuan Lin [11] proposed a combined AHP and TOPSIS method to define consumer needs for the effective assessment of design solutions. The main disadvantage of this method is the rigorous mathematical steps involved and the task of assigning a relative weightage for each attribute. MCDM methods are also used for the selection of PCMs for applications such as waste heat recovery [12] and thermal comfort of vehicle occupants [13]. Rastogi et.al [14] evaluated different PCMs for their thermal performance in HVAC applications and ranked them using MCDM techniques. The TOPSIS and Ashby approaches were used to rank the PCM, and the best candidate was decided as RUBITHERM GmbH-SP 24E. Wang et al. [15] selected the optimum phase change material for a low-temperature TES system using the AHP – VIKOR method. The relative weightage of each property was evaluated by the AHP method and ranked different PCMs using the VIKOR method. Stearic acid was found to be optimal PCM among the candidates for low-temperature thermal energy storage. Maniya and Bhatt [16] introduced the Preferred Selection Index (PSI) method as an MCDM tool to assist decision-makers in selecting the suitable material for the design. Unlike the other MCDM methods, the PSI method does not need to determine the relative importance between attributes. From the literature review, it is clear that the selection of a suitable PCM is an important step in designing a phase change energy storage (PCES) unit. Though a few researchers have recognized the use of MCDM techniques in the selection of heat storage materials, their performance analysis on a PCES device is rarely seen. Furthermore, the use of the PSI method needs to be explored in detail to make the selection of PCM easier and comprehensive.

The low thermal conductivity of PCMs is the main reason for long charging and discharging time. Employing fins is the well-established way to increase the heat transfer rate in the melting/solidification process and hence reduces the charging/discharge time [17–20]. However, the shape of the fins and their orientation is also important. Murray et al. [21] experimentally studied a PCES unit integrated with the fin and reported that the presence of natural convection during the melting process is related to the position of fins. Abdulef et al. [22] presented a detailed review of various shapes and geometrical arrangements of the fins, such as circular, longitudinal, pin, and plate fins, which are commonly used to enhance thermal performance. The study narrates that the longitudinal and circular fins have better thermal performance compared to pin fins and plate fins. An experimental study conducted by Mahta et al. [23] evaluated the performance of spiral fins in a vertical heat storage unit. The study inferred that the installation of a spiral fin can effectively reduce the total cycle time by 31.82% however the manufacturing time and cost seem to be its downsides. Mahdi et al. [24] conducted a numerical and experimental study to investigate the effect of orientation of LHS unit. The study examined the performance of finned and non-finned LHSU in horizontal and vertical orientation. The results suggest that the addition of fins reduces melting time by 50%. Although the non-finned LHSU performs well in the horizontal orientation, the orientation has a minor impact on the finned LHSU. Sheikholeslami et al. [25] numerically studied the effect of copper oxide nanoparticles and V-shaped fins in the solidification process of PCM. Parameters like concentration of nanoparticles, angle of V-shaped fin, size and length of fins are varied to obtain the optimal design. In addition, the design of the PCES device with proper fin shapes plays a significant role in heat transfer enhancement. [18,21] Most of the studies focused on the effect of vertical and horizontal plate-fin on charging/-discharging time. However, the optimisation of fin shape is important. The design of fins is to be in such a way that it will not hinder the natural convection current [21]. It is expected that the PCES unit with an optimum fin configuration can be a wiser choice for solar adsorption cooling systems as it reduces the material cost and size of the whole system.

The present study, for the first time, examined the feasibility of using the PSI method to select a PCM suitable for the heat storage unit. The PCM selected using the PSI method is stacked inside the newly designed PCES unit to evaluate its overall performance. The structured outline of the design process is shown in Fig. 1. The selection process comprises a pre-screening process and the ranking of PCMs. The top-ranked PCM is used in a cylindrically encapsulated PCES unit for its performance evaluation. ANSYS 2020R1 software is used for numerical analysis,

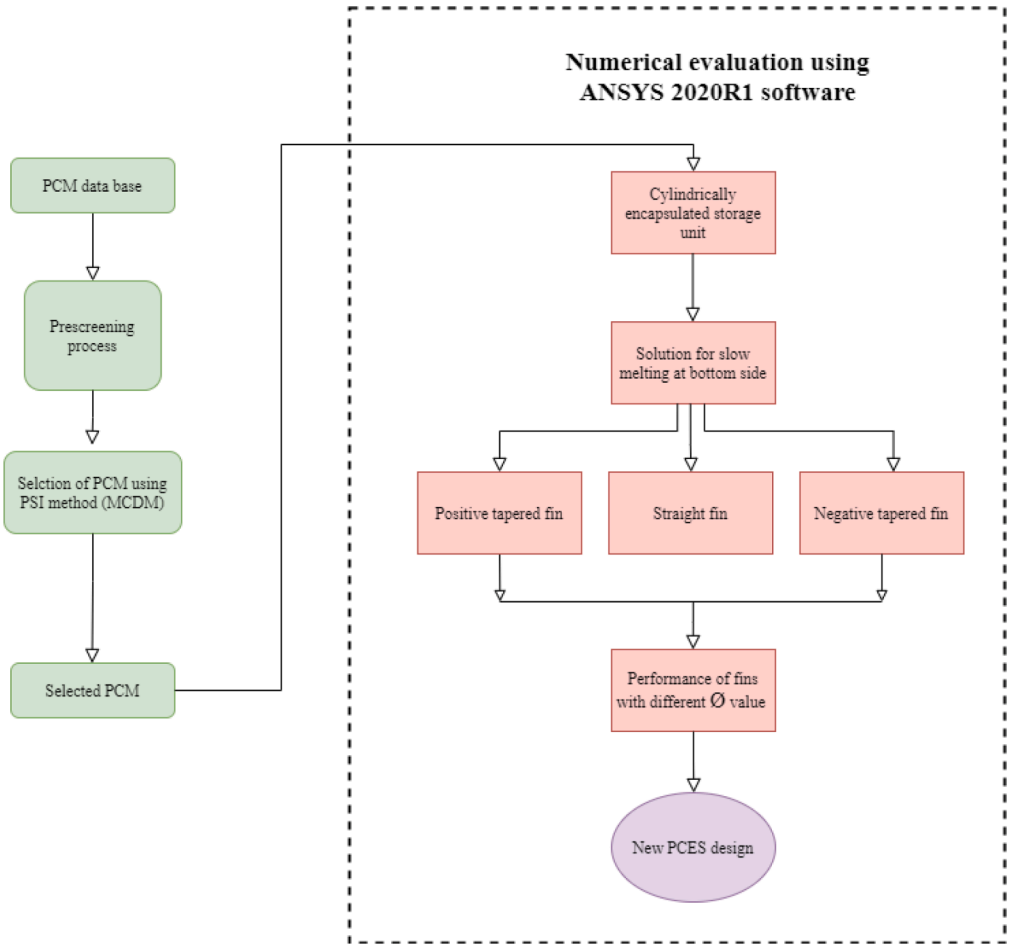

Fig. 1. Flow chart of New PCES unit design.

which involves the evaluation of system performance at three different fin shapes, namely, positive tapered, negative tapered, and zero tapered. Finally, an optimization study is performed by changing the taper parameter of the fin. The study also examines the real-world performance of the designed PCES unit by considering the case study of a solar vapour adsorption chiller situated in Taiwan.

2. Material assessment and the design of PCES unit

Preference Selection Index (PSI) method is used here for ranking the PCMs based on their thermophysical properties and cost. The desired desorption temperature of the SAC system is 60 °C-150 °C for commonly used working pairs. Since phase transition temperature is one of the important parameters for selecting PCM, a pre-screening process is required to select suitable materials for it. Adsorption chillers use activated carbon and methanol [6], or activated carbon-ethanol typically needs at least 75 °C as inlet temperature to achieve better desorption. A temperature gradient of 10 °C is to be maintained in between the TES and the adsorption bed. The melting temperature, density (ρ), enthalpy of fusion (H_f), specific heat (C_p), and thermal conductivity (k) are some of the key parameters that determine the performance of a PCES system. Material with a high enthalpy of fusion can provide high energy storage density. Good thermal conductivity reduces the melting-solidification time, and high density reduces the size of the PCES system. Thermal stability of PCMs is an important factor, as it ensures that the melting temperature and enthalpy of fusion do not change significantly over time. The majority of commercial PCMs possess good thermal stability up to 1000 cycles. Thermal stability also depends on the operating temperature, and after a specific temperature limit (degradation temperature), materials may lose their thermophysical qualities [26]. The maximum operating temperature (T_{max}) within which the PCM possesses thermal stability is also considered as one of the selection criteria in the present work. The cost of the phase change material (C) is an important factor that needs to be included in the selection of PCM. Thermophysical properties and cost of different PCMs considered for the present investigations are listed in Table 1.

2.1. Preference selection index methodology

The PSI method uses the overall preference value to rank PCM materials. It doesn't need the relative weightage between attributes and hence it is advantageous when the relative weight between attributes is difficult to find out. With overall preference value, preference selection index (PS_I) for each alternative is determined, and the one with the highest PS_I value is considered the best alternative. The methodology of PSI [16,32] is explained in the following steps.

Step I: Decision matrix

First, a decision matrix A is formulated by arranging attributes (properties) in the columns and alternatives (different PCMs) in the rows. Mij is the performance of alternatives as illustrated in Table 2. Attributes are classified into two types, namely, beneficial attributes and non-beneficial attributes. The cost of PCM is considered as a non-beneficial attribute, and all other properties are considered as beneficial attributes.

Step II: Normalization matrix

Table 1
Thermophysical properties of different PCMs used.

Sl.No	PCM Name	T_m(K)	H_f(KJ kg^{-1})	ρ(kg m^{-3})	Cp(kJ.kg^{-1}.K^{-1})	T_{max}(K)	K(W/mK)	C(€)	Ref.
PCM1	PlusICE S89	89	145	1550	2.48	120	0.67	17.45	[27]
PCM2	SavE HS89	88	188	1630	2.65	95	0.65	01.92	[28]
PCM3	RT 90HC	91	140	950	2.00	120	0.20	18.06	[29]
PCM4	PlusICE A95	95	260	900	2.20	300	0.22	34.91	[27]
PCM5	RT 100	100	90	880	2.00	120	0.20	06.48	[30]
PCM6	PlusICE H105	100	125	1700	1.50	390	0.50	40.71	[27]
PCM7	RT 100HC	114	150	1000	2.00	130	0.20	09.24	[31]
PCM8	PlusICE S117	117	125	1450	2.61	140	0.70	17.45	[27]
PCM9	PlusICE A118	118	195	900	2.20	250	0.13	34.91	[27]

Table 2
Decision matrix model.

		Attributes				
		P_1	P_2	P_3	P_4	…P_n
Alternatives	A_1	M_{11}	M_{12}	M_{13}	…	M_{1m}
	A_2	M_{21}	M_{22}	M_{23}	…	M_{2m}
	...	:	:	:	:	:
	A_n	M_{n1}	M_{n2}	M_{n3}	…	M_{nm}

After normalizing matrix A, its element values transform into a range of 0–1. For beneficial attributes, the normalization is done by

$$C_{ij} = \frac{M_{ij}}{M_j^{max}} \tag{1}$$

For non-beneficial attributes, the normalization is done by

$$C_{ij} = \frac{M_{ij}}{M_j^{min}} \tag{2}$$

The obtained data is given in Table 3.

Step III: Calculate preference variation (ωj)

For each element, a preference variation value (ωj) is defined using the following equation:

$$\omega_j = \sum_{i=1}^{n} \left[M_{ij} - \overline{M_j}\right]^2 \tag{3}$$

The term preference variation value symbolizes the Euclidean distance between the normalized and the average normalized attributes [33]. $\overline{M_j}$ is the mean of normalized value of element j and it is given by

$$\overline{M_j} = \frac{1}{N}\sum_{i=1}^{n} M_{ij} \tag{4}$$

Table 4 shows the preference variation of different PCMs used.

Step IV: Overall preference value (Ψj)

In this step the overall preference value (Ψj) is calculated for each element. Deviation (θj) is determined from the following equation

$$\theta j = 1 - \omega_j \tag{5}$$

where $\omega_j$is the preference variation is calculated using Eq. (3)

Then the overall preference value $\Psi_j$has been obtained by

$$\Psi_j = \frac{\theta_j}{\sum_{j=1}^{m}\theta_j} \tag{6}$$

The total overall preference value of all the properties should be one, i.e. $\sum_j \Psi_j = 1$

The calculated value of overall preference of attributes are tabulated in Table 5

Step V: Obtain preference selection index (PSI).

The preference selection index (PSi) for each alternative is computed by using the following equation:

$$PS_I = \sum_{j=1}^{m}\left(M_{ij} \times \Psi_j\right) \tag{7}$$

Step VII: Ranking each alternative

Now the alternatives are ranked according to the descending order of the PS_I. The alternative with the highest PSI value is ranked as 1 and the alternative with the least value is considered as the least performing one.

The overall rank of each attribute is given in Table 6. From the study, it can be concluded that the SavE-HS89 (PCM-9) is the PCM with better properties and the least performing one is RT100 (PCM-2). The overall weightage of PCMs is shown in Fig 2. It is clear from Fig. 2 that the SavE-HS89 has better weightage as compared to the second-ranked PCM (PlusICE A95). Also, the technical data sheet published by the manufacturer indicates that the top-ranked material possesses good thermal stability up to 1000 thermal cycles [28].

2.2. Validation of the PSI method

To ensure the credibility of the PSI method, the results are compared with another widely used MCDM technique, AHP-TOPSIS. Researchers

Table 3
Normalised data matrix.

Sl. No	PCM Name	H_f	ρ	Cp	T_{max}	k	C
PCM1	PlusICE S89	0.5577	0.9118	0.9358	0.3077	0.9571	0.1100
PCM2	SavE HS89	0.7231	0.9588	1.0000	0.2436	0.9286	1.0000
PCM3	RT 90HC	0.5385	0.5588	0.7547	0.3077	0.2857	0.1063
PCM4	PlusICE A95	1.0000	0.5294	0.8302	0.7692	0.3143	0.0550
PCM5	RT 100	0.3462	0.5176	0.7547	0.3077	0.2857	0.2963
PCM6	PlusICE H105	0.4808	1.0000	0.5660	1.0000	0.7143	0.0472
PCM7	RT 100HC	0.5769	0.5882	0.7547	0.3333	0.2857	0.2078
PCM8	PlusICE S117	0.4808	0.8529	0.9849	0.3590	1.0000	0.1100
PCM9	PlusICE A118	0.7500	0.5294	0.8302	0.6410	0.1857	0.0550

Table 4
Preference variation value.

Sl. No	PCM Name	Hf	ρ	Cp	Tmax	K	C
PCM1	PlusICE S89	0.0023	0.0382	0.0126	0.0278	0.1651	0.0123
PCM2	SavE HS89	0.0137	0.0588	0.0312	0.0533	0.1427	0.6071
PCM3	RT 90HC	0.0046	0.0248	0.0047	0.0278	0.0703	0.0131
PCM4	PlusICE A95	0.1552	0.0349	0.0000	0.0869	0.0559	0.0275
PCM5	RT 100	0.0675	0.0395	0.0047	0.0278	0.0703	0.0057
PCM6	PlusICE H105	0.0157	0.0805	0.0663	0.2763	0.0267	0.0302
PCM7	RT 100HC	0.0008	0.0164	0.0047	0.0199	0.0703	0.0002
PCM8	PlusICE S117	0.0157	0.0187	0.0261	0.0133	0.2018	0.0123
PCM9	PlusICE A118	0.0207	0.0349	0.0000	0.0278	0.1333	0.0275

Table 5
Overall preference value of each attribute.

	Hf	ρ	Cp	Tmax	K	C
Preference value	0.2366	0.2197	0.2857	0.1477	0.0214	0.0888

confirm the validity of the combined AHP-TOPSIS method for choosing PCM in heat storage applications [12,34].The ranking of PCMs obtained based on PSI and the AHP-TOPSIS method is presented in Fig. 3.

From the figure, it is clear that both PSI and AHP-TOPSIS methods suggest PCM9 (SavE-HS89) as the best one with rank 1. The ranks of each PCMs by the combined AHP-TOPSIS method is obtained as PCM-2> PCM-4> PCM-1> PCM-8> PCM-9> PCM-7> PCM-6> PCM-3> PCM-5 whereas by the PSI method it is PCM-2> PCM-4> PCM-1> PCM-8> PCM-6> PCM-9> PCM-7> PCM-3> PCM-5. The ranks of PCM-1, PCM-2, PCM-3, PCM-4, PCM-5 and PCM-8 obtained by both methods are 3, 1, 8, 2, 9 and 4, respectively. It suggests the efficiency of PSI method, and hence it is recommended. The process of assigning a weightage of each attribute is eliminated in PSI, and hence it reduces the computation time without compromising its accuracy. This makes PSI a favourable method for selecting PCMs for solar cooling systems compared to the conventional AHP-TOPSIS method.

3. Numerical model of PCES unit

3.1. System description and governing equations

Use of fins is the most economical and effective way to improve the thermal performance of a storage unit. The position and shape of fins play a vital role in the design part of PCES. The previous studies summarised that [21], the position of a fin should not hinder the natural convection current. In this study, a tapered vertical fin design is employed to compensate the slow melting at the bottom region, and also it does not offer a surface that obstructs natural convection currents. Tapered vertical fins with three different taper angles, namely, positively tapered, negatively tapered and zero tapered fins are arranged around the periphery of the inner pipe as shown in Fig. 6 is considered for the present study. Total 12 fins are placed radially at an equal distance. The encapsulation with 100 mm diameter is taken for the PCES.

Table 6
Overall rank of each alternative.

Sl.No	PCM Name	H_f	ρ	Cp	T_{max}	K	C	PSI	Rank
PCM1	PlusICE S89	0.1320	0.2003	0.2674	0.0454	0.0205	0.0098	0.67538	3
PCM2	SavE HS89	0.1711	0.2107	0.2857	0.0360	0.0199	0.0888	0.81218	1
PCM3	RT 90HC	0.1274	0.1228	0.2156	0.0454	0.0061	0.0094	0.52684	8
PCM4	PlusICE A95	0.2366	0.1163	0.2372	0.1136	0.0067	0.0049	0.71538	2
PCM5	RT 100	0.0819	0.1137	0.2156	0.0454	0.0061	0.0263	0.48916	9
PCM6	PlusICE H105	0.1138	0.2197	0.1617	0.1477	0.0153	0.0042	0.66237	5
PCM7	RT 100HC	0.1365	0.1292	0.2156	0.0492	0.0061	0.0185	0.55520	7
PCM8	PlusICE S117	0.1138	0.1874	0.2814	0.0530	0.0214	0.0098	0.66676	4
PCM9	PlusICE A118	0.1775	0.1163	0.2372	0.0947	0.0040	0.0049	0.63453	6

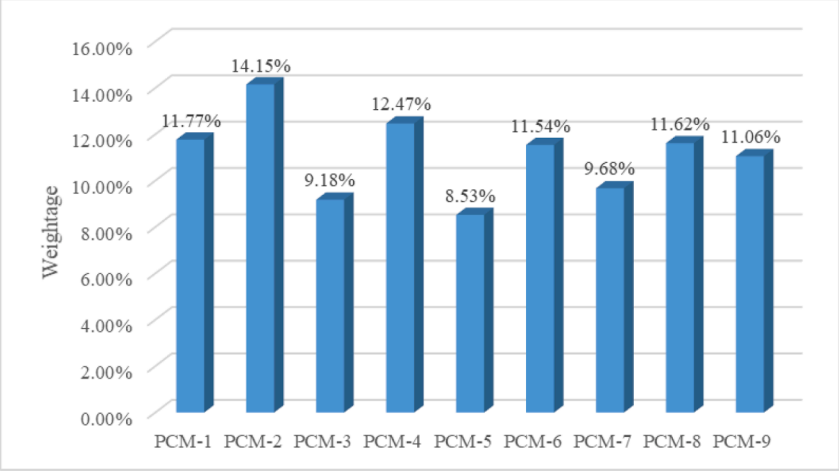

Fig. 2. The overall weightage of each PCM by considering its preference selection index.

	PCM-1	PCM-2	PCM-3	PCM-4	PCM-5	PCM-6	PCM-7	PCM-8	PCM-9
AHP-TOPSIS	3	1	8	2	9	7	6	4	5
PSI	3	1	8	2	9	5	7	4	6

Fig. 3. Comparative ranking of the PCMs by different MCDM methods.

Water at 2 bar pressure is used as the Heat Transfer Fluid (HTF) and is circulated through the inner tube of diameter 28 mm. Annular space is filled with the PCM selected by the PSI method. Straight fins with dimensions 17×2 × 500 mm are used as a reference model (Figs. 4 and 6a) and the performance of new fin shapes are compared with it.

Numerical modelling is carried out with the following assumptions:

(i) The PCM is homogeneous and isotropic
(ii) Thermophysical properties are constant in each phase except the density
(iii) PCM is bounded by an adiabatic wall
(iv) Thermal stresses are ignored

The numerical model solves the Energy, momentum and continuity equations in the relevant domain. Governing equations for the combined conduction and convection melting phenomenon used are as follows:

Continuity equation:

$$\frac{\partial \rho}{\partial t} + \nabla.\left(\rho \vec{V}\right) = 0 \tag{8}$$

Momentum equation:

$$\frac{\partial\left(\rho \vec{V}\right)}{\partial t} + \nabla.\left(\rho \vec{V}\right) = -\nabla p + \mu \nabla^2 \vec{V} + \rho g + S_x \tag{9}$$

Energy equation:

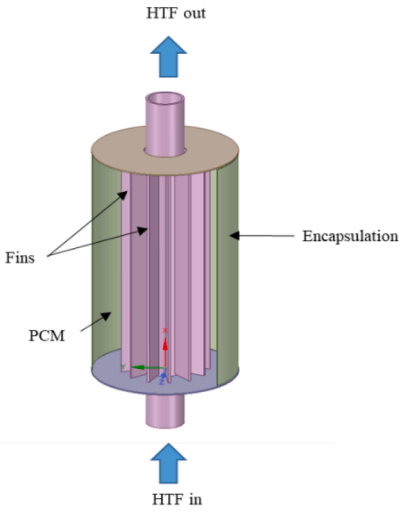

Fig. 4. Schematic diagram of PCES unit with vertical fins.

$$\frac{\partial(\rho H)}{\partial t} + \nabla.(\rho v H) = k\nabla^2 T \tag{10}$$

where H is the total enthalpy term

$$H = h + \Delta H \tag{11}$$

where

$$h = h_{ref} + \int_{T_{ref}}^{T} C_p dT \tag{12}$$

$$\Delta H = fL \tag{13}$$

h_{ref} in the Eq. (12) represents the enthalpy of the material at a reference temperature, T_{ref} and L are the latent heat of fusion of PCM. The term *f* represents the liquid fraction, which varies between 0 and 1 during charging (melting process), and is defined as follows:

$$f = \begin{cases} 0; if\ T < T_s \\ \dfrac{T - T_s}{T_l - T_s}; if\ T_s < T < T_l \\ 1; if\ T > T_l \end{cases} \tag{14}$$

The source term in the last part of the momentum Eq. (9) is expressed as

$$S_x = \frac{(1-f)^2}{(f^3 - \varepsilon)} A_{mushy} \tag{15}$$

where ε is a small number(0.001) added to the denominator of the Eq. (15) to avoid division by zero when the value of f tends to zero. A_{mushy} is the mushy zone constant (10^5), indicating how steeply the velocity is reduced to zero when solidification occurs. The effect of natural convection is also considered by using the Boussinesq approximation:

$$\rho = \rho_l(1 - \beta(T - T_m)) \tag{16}$$

where $T_m = (T_l + T_s)/2$

This melting-solidification model is solved by using the Navier-stokes equations, which uses the enthalpy- porosity technique.

The energy and momentum Eqs. (8) to (10) are solved by using a second-order upwind scheme. Semi-implicit pressure-linked equation (SIMPLE) is employed for pressure and velocity coupling. PRESTO scheme is applied for pressure correction. The second-order differencing scheme is selected for discretization. A grid independence study is conducted with 332,561, 415,283, 658,931, and 826,512 elements and grid size with 415,283 elements are selected. It can be found that further

refinement of mesh could not make any notable progress in the accuracy of the result. Fig. 5(a) represents the top view of the PCES unit after meshing. Only a sector of PCM-fin domain is considered for the analysis, as it reduces the computation cost. Periodic boundary conditions are used on either side of the PCM domain to understand the overall system behaviour. Polyhedral meshing is used here, and more refinement in meshing is provided on the solid-fluid interfaces. The time step value is fixed as 0.1 s and the convergence criteria of 10^{-4}, 10^{-4}, and 10^{-6} are selected for continuity, momentum, and energy equation, respectively.

4. Results and discussion

Mathematical modelling of a PCES system integrated with different fin shapes is presented here. The performance of positive and negative fins are studied and are then compared with the straight fin. The numerical modelling of the system is carried out in the ANSYS2021 environment with the baseline parameters given in Table 7.

The initial temperature of the PCM is taken as 300 K, and inlet temperature and velocity of hot HTF are set to 369 K and 0.15 m/s, respectively. The fin surface area is fixed as 18,000 mm^2 for all cases studied. The tapered fin's dimensions are chosen based on the Eq. (17).

$$y = (R - r) \times \varnothing \tag{17}$$

The term Ø is introduced here as the fin parameter, which is defined as the extent to which the fin length is selected through the distance R-r as shown in Fig. 6(b). Value of fin parameter, is taken as 90%, 80%, 70%, 60% and 50% to optimise the taper angle. The value of 'y' increases with Ø and the corresponding 'x' value decreases. The value 'y' with $\varnothing = 90\%$ is used to represent a positive tapered fin, while the value 'y' with 1-Ø represents a negative tapered fin. The value of Ø is fixed at 50% for zero tapered fins.

4.1. Validation of the numerical model

The numerical model is validated with the experimental study conducted by Akgun et al. [35]. The experimental data that correspond to the evolution of temperature at point T61 are compared with the numerical results, as shown in Fig. 7.The results show a good agreement between numerical and experimental results. Validation of the numerical model is confirmed by calculating the correlation coefficient (c) [36], which determines the deviation of numerical results from the experimental values.

$$Correlation\ coefficient = \frac{n\sum x_i y_i - (\sum x_i)(\sum y_i)}{\sqrt{n\sum x_i^2 - (\sum x_i)^2}\sqrt{n\sum y_i^2 - (\sum y_i)^2}} \tag{18}$$

where 'x' is the numerical result and 'y' is the experimental result. The correlation coefficient is calculated as 0.92 and hence the model is acceptable.

4.2. Effect of tapered fin design configuration

At the beginning of the charging process, heat supplied by the pipe wall is absorbed by the PCM as sensible heat. Once the temperature approaches the melting point of PCM, a significant amount of heat from the pipe surface is used for the phase transition process. The layer of melted PCM rises as buoyancy-driven convection strengthens during the melting progress. The solid-liquid interface region absorbs heat from the hot melted PCM for its phase transition. As a result, the temperature of molten PCM drops, and density increases, causing its downward movement. Thus, when compared to the lower part, the melting rate is more predominant in the top part and due to this, the melt interface becomes noticeably curved. Fig. 8 depicts the contours of melt fraction for negative taper, positive taper, and zero taper fins at 3000 s, 4000 s, 7000 s, and 12000s, respectively. Initially, the melting is more rapid in the top region in the positive tapered fin as compared to the negatively tapered fin. As the melting progresses, the convection current establishes, and hence, faster melting is noticed in negatively tapered fins in the later stages.

4.2.1. Enhancement in charging time

Charging time is a significant parameter of a thermal energy storage system, and it is defined as the time taken for the system to store heat energy to the limit at which it is designed. Quick charging-discharging provides a consistent temperature output regardless of the load fluctuations. The time required to completely liquefy PCMs (melt fraction =1) of the proposed PCES model with three shapes, namely, positive tapered, straight and negative tapered is shown in Fig 9. It is clear that charging time reduces in negatively tapered fins compared with positive fin and zero fins. The charging time for the negatively tapered fin is 12,100s whereas it is 19,000s and 13,900s for positively tapered and zero tapered fins (straight fin), respectively. The negatively tapered fin shows a 13% reduction in melting time as compared to the straight fin, and it is 36% in comparison with the positively tapered fin. The lower surface area of the positively tapered fin at the bottom region of PCM results in a longer charging time. Also, the charging time of straight fins is in between the positive and negative tapered fins due to their moderate exposed surface area.

4.2.2. Variation in total stored energy of PCES unit

The total energy stored (E_T) in the phase change material is the sum of sensible heat(E_S) and latent heat (E_L).

$$E_S = m.C_p.(T_{initial} - T(t) \tag{19}$$

where m is the mass of PCM domain and Cp,the specific heat at constant pressure,T(t) the average temperature of the PCM at time t

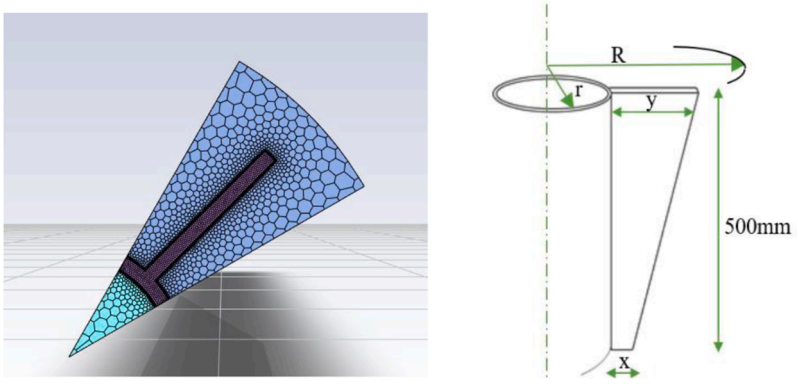

Fig. 5. (a) Sector of the cylindrical section of PCES after meshing (b) Schematics of fins.

Table 7
Baseline parameters.

Region	Outer wall	Sidewall	Inlet condition	Outlet condition	Initial temperature
Boundary condition	Insulated boundary	Periodic boundary	Velocity inlet 0.05 m/s, 369K	Pressure outlet	300K

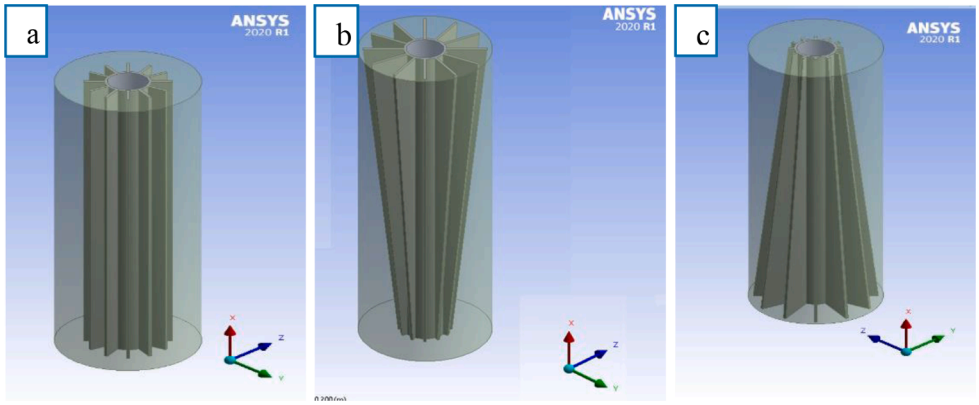

Fig. 6. Fin geometries (a) straight fin with zero taper angle (b) negatively tapered fin (c) positively tapered fin.

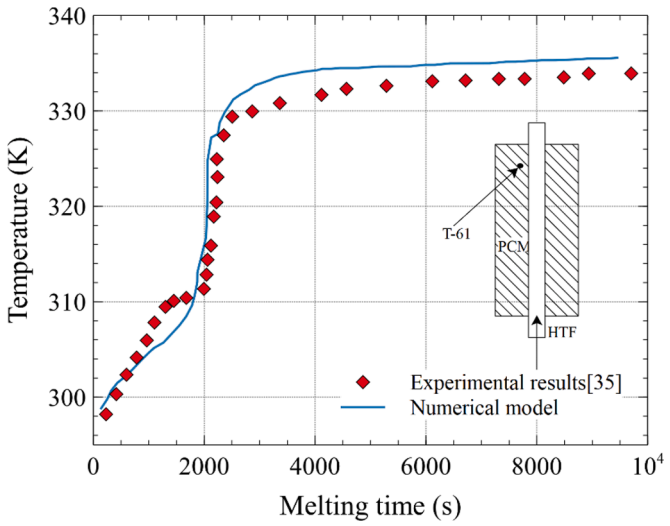

Fig. 7. Comparison of numerical results with experimental values inside PCM.

$$E_L = m.H_{fg}.f(t) \tag{20}$$

where H_{fg} is the enthalpy of fusion of the material and $f(t)$ the temporal variation of melt fraction.

$$E_T(t) = E_s + E_L \tag{21}$$

The total amount of stored energy in the system is directly proportional to the mass fraction and overall temperature rise in the phase change material. The temporal variations of the total energy stored is presented in Fig. 10. In the beginning, energy received from the heat transfer fluid is used for the sensible heating of PCM, and it raises the bulk solid temperature. After that, the material reaches its melting point and tends to absorb latent heat (enthalpy of fusion). This causes a significant change in the overall stored energy as shown in the Fig. 10. Once the whole PCM is melted, the energy absorbed from the heat transfer fluid is used for sensible heating of liquid PCM. This sensible heat stored after complete melting of PCM is comparably small, and hence the storage curve flattens. The rise in stored energy is greater for straight fin PCES unit than negative fin-type until about 7000 s, as it provides a uniform heat transfer area. During the further stage of melting, the negatively tapered fins gathers more heat energy than a straight fin design because of the combined conduction-convection effect. In positive tapered fins, the conduction heat transfer at the bottom and subsequent melting are small in comparison with the other two, so the latent heat stored over a given period is lower, resulting in less overall stored energy value.

4.2.3. *Variation in heat flux*

The temporal variation of heat flux for three different fin configurations considered are depicted in Fig. 11. Initially, the value of heat flux is very high in all cases, as the temperature difference between the heat transfer fluid and PCM is very high over a small distance. Due to this high heat flux at the beginning, the PCM melts on the pipe wall surface. This melted PCM will attains the temperature as comparable to the pipe walls, provides a thermal resistance, and hence the heat flux decreases sharply. Later, buoyancy-driven convection streams are formed, which stabilizes the heat flux as shown by the horizontal region of the curve in Fig. 11. The heat flux in this region is not significant in positively tapered fins as compared to the other two cases due to its low heat transfer rate at the bottom region. The negatively tapered fins with the higher heat transfer area at the bottom region creates a combined conduction-convection effect and thereby increases the overall heat flux.

4.2.4. *Geometrical optimization of negative tapered fin*

The present study reveals the merits of a negatively tapered fin in comparison with the straight fin and positively tapered fins. Geometrical optimization of the PCES unit is important for its practical design. The study of variations of melt fraction and charging time with Ø is helpful for optimising the PCES unit. The value of Ø is varied from 50% to 90% and the change in melt fraction and charging time is plotted in Fig. 12. It requires melting time of 13,900s, 13,320s, 12,400s, 12,210s, and 12,100s for fin parameter of 50%, 60%, 70%, 80%, and 90%, respectively for the complete melting of PCM. It is evident that the minimum charging time obtained is for a fin with Ø value of 90%, as it provides the maximum surface area at the bottom region. The performance of these fins is not consistent during the melting process. The fin with Ø value of 80% leads the melting process during the first half of the overall melting period. Considering all these factors, the optimization of the fin parameter is evaluated and is represented in Fig. 13. It can be seen that the charging time reduces drastically from 50% to 70% and thereafter it is almost constant. This is due to the reduction in heat conduction area at the top part of the fin compared to the bottom portion. The optimised

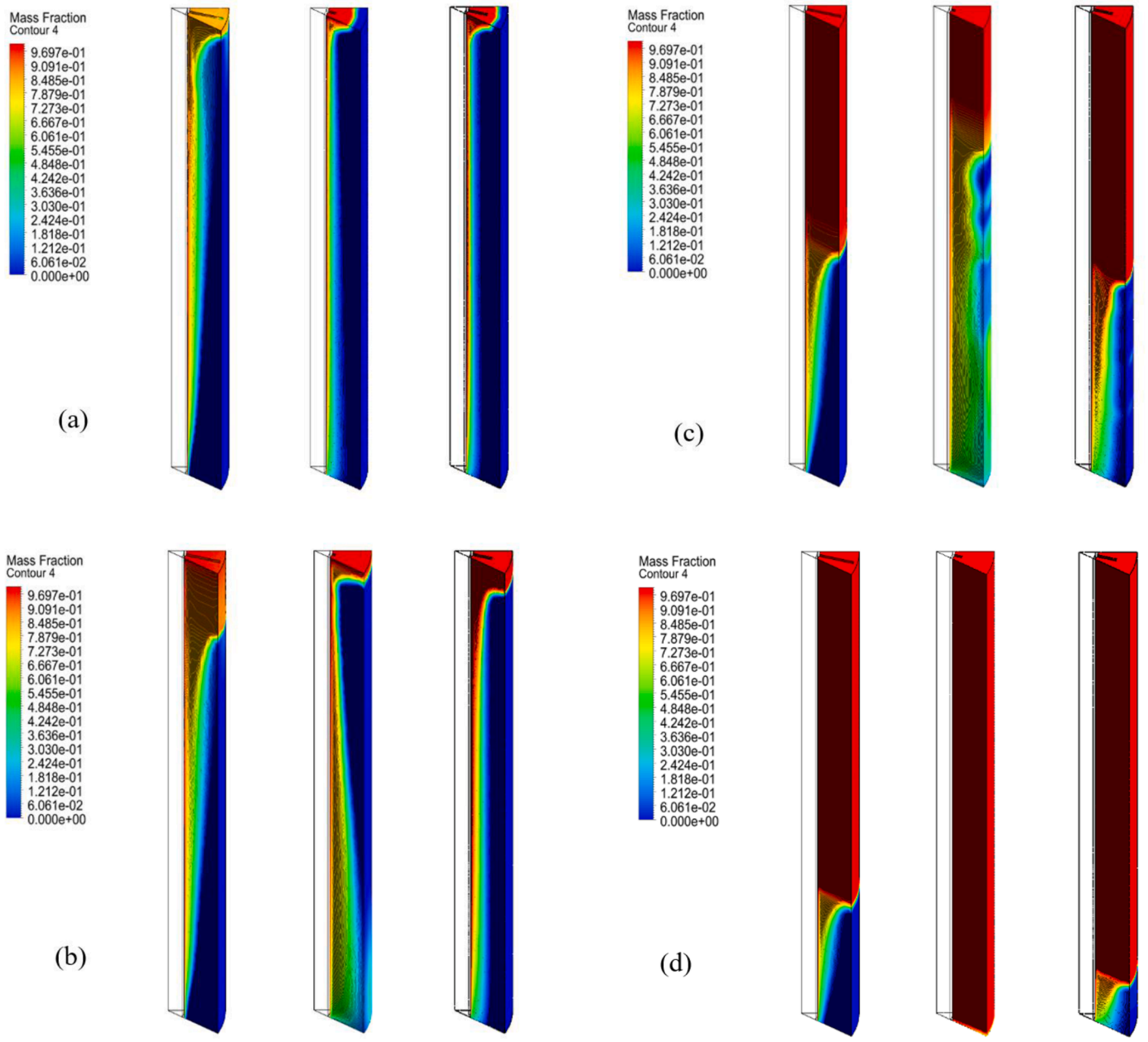

Fig. 8. Contours of melt fraction for positive taper, negative taper and zero taper fin at a)3000 s, b)4000 s, c)7000 s, and d)12000s.

value of Ø is taken as 80% and the value of 'y' is taken as 27.2 mm.

4.2.5. Effect of flow Reynolds number on melting time

The influence of flow velocity of HTF on overall melting time is represented in Fig. 14. The Reynolds number varies from 2252 to 22,520 at the constant inlet temperature. The reduction in melting time is noticed with the increase in Reynolds number. This is due to the formation of turbulence, which causes an increase in heat transfer rate. The melting time decreases by 45% when the Reynolds number changes from 2252 to 15,000. However, after 15,000, there is no noticeable decrease in melting time. Hence, the further increase in the flow velocity of HTF is ineffective for improving the heat transfer. It is clear that the flow velocity of HTF has a significant impact on the thermal efficiency of the PCES unit.

5. Case study of a 10KW solar adsorption chiller integrated with proposed PCES unit

Adsorption chillers have gained considerable attention in the last two decades due to their ability to use low-grade energy such as solar energy within the temperature ranging from 60 °C-150 °C. Furthermore, these types of chillers are free from noise, less maintenance and are easily controllable. The low performance and intermittency are the main obstacles for the commercialisation of solar adsorption cooling systems. The intermittency in the working cycle of SAC can be eliminated by integrating it with a sensible heat storage system (currently employed practise) or by a highly efficient latent heat storage system. The performance study of the proposed PCES unit is carried out by integrating it with a SAC system of 10 kW capacity, which is located at Taiwan's Industrial Technology Research Institute [37]. The chiller is employed with a sensible heat storage (hot water storage tank) to eliminate the temperature fluctuations. The schematic diagram of the two-bed

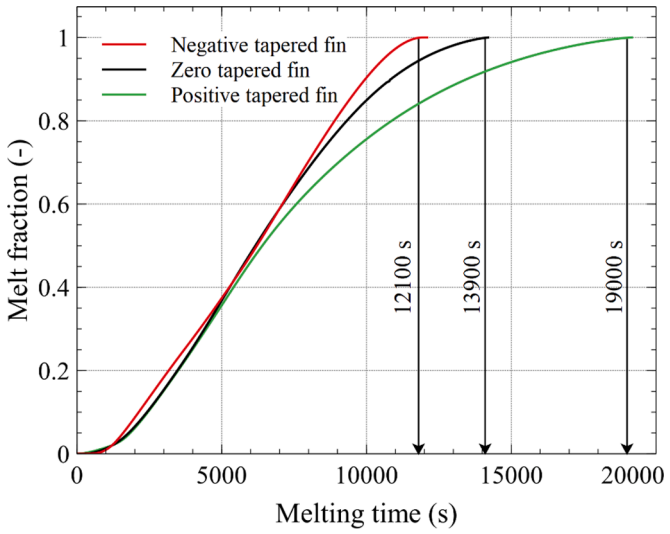

Fig. 9. Variation of mass fraction with melting time for three different fin shapes.

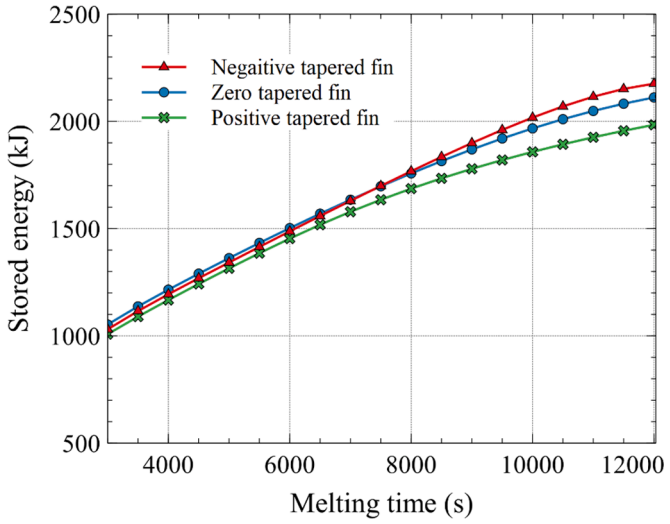

Fig. 10. Variation of stored energy with charging time for three different fin shapes.

adsorption chiller developed by Chang in Hsinchu, Taiwan [37] is shown in Fig. 15. The system comprises an array of solar collectors, an adsorption chiller and a cooling tower. The working material used is silica gel-water. The installed solar collector is capable of raising the water temperature up to 90 °C. The COP of the system reported is 0.37.

In the present study, the proposed PCES unit stacked with selected PCM (SaveHS-89) and negatively taped fins is integrated to the chiller to replace the conventional hot water storage tank. At a full load of 10 kW, the total heat required by the chiller is 27 kW (at COP of 0.37). It is assumed that the total rate of heat absorption during melting is equal to the heat released to HTF through PCM solidification. The sensible heat, latent heat, and total heat stored/released per hour for the single module (single pipe in pipe unit) are obtained and is shown in Table 8. Each PCES module contains 5.745 kg of SavE HS89-PCM and each kilogram costs 2.02€. The total amount of heat stored or released by the single module is found to be maximum for a negatively tapered fin, and it is about 640 kJ/h. The high rate of heat storage/release makes it a favourable choice which reduces the overall requirement of PCM.

The number of units required to deliver heat for 3 h (from 11:00 to 14:00) of storage is calculated. It is observed that 202 units of straight-

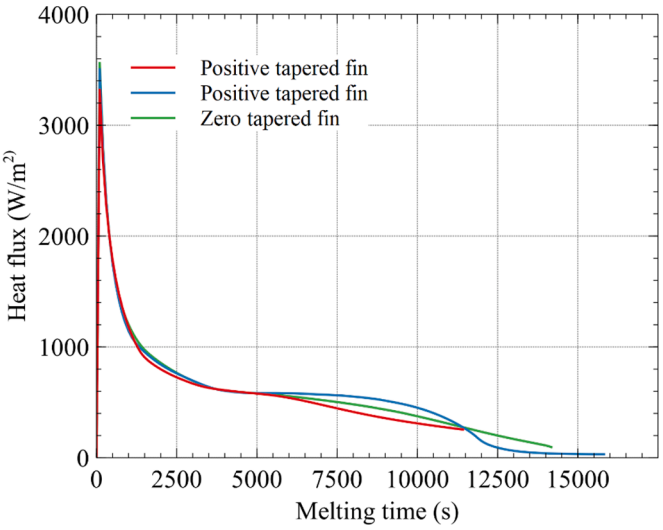

Fig. 11. Temporal variation of heat flux for three different fin shapes.

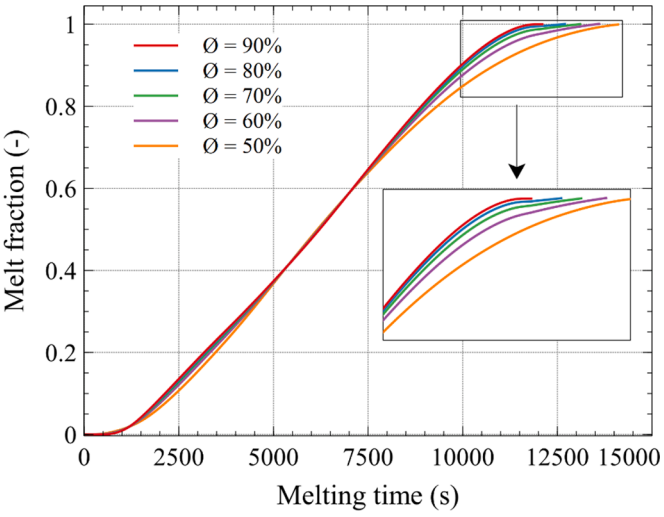

Fig. 12. Temporal variation of melt fraction for different Ø value.

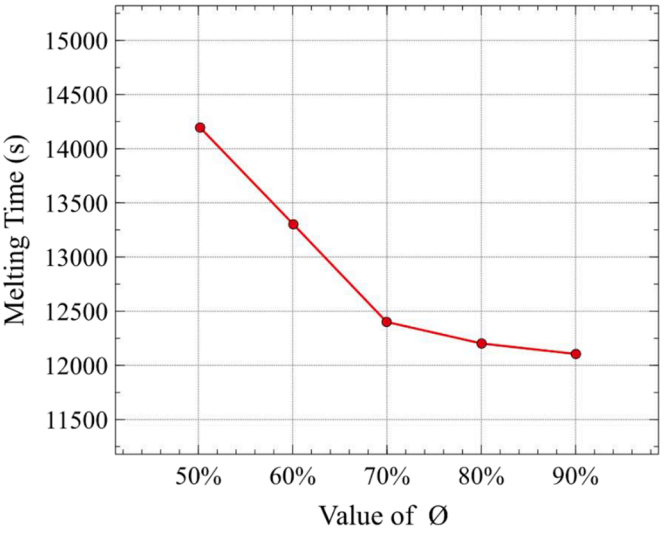

Fig. 13. Temporal variation of charging time for three different Ø value.

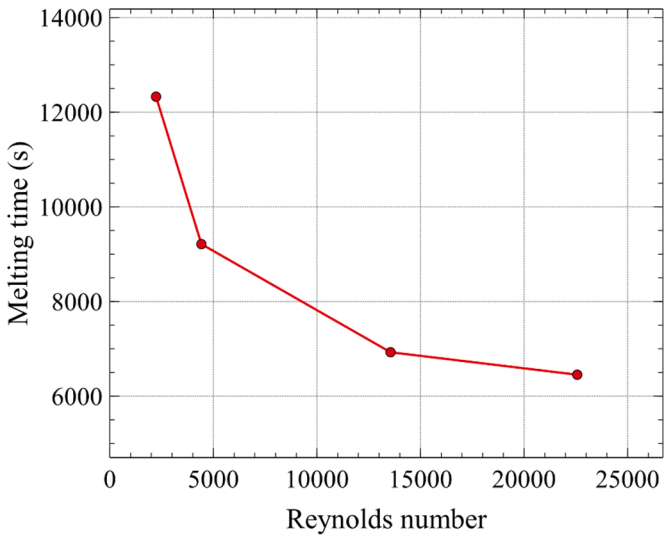

Fig. 14. influence of flow velocity on melting time.

fin PCES module are required for the adsorption chiller. The required number of PCES units having negatively tapered fins is only152, which is about 25% less as compared to the previous case. By using the new design the cost of the entire heat storage system can be minimized. The expenses of steel and HTF are neglected for the calculation as it is not significant in comparison with the cost of PCM. The new PCES unit with negatively tapered fins can reduce 46% of the total cost as compared with the storage without fins. Hence the proposed design with fewer units makes the solar adsorption cooler a compact one.

6. Conclusions

The present study proposes a highly efficient PCEs unit with negatively tapered fin for solar adsorption cooling systems. The study also intends to rank different commercially available phase change materials based on their thermophysical properties for the design of storage system. The top-ranked material is used inside the proposed PCES unit for the performance assessment. The conclusions derived from the present study are as follows:

(a) PSI method is proven to be an alternative for conventional AHP-TOPSIS method for the selection of PCM for solar cooling systems and their applications. PSI method is used to rank different PCMs commercially available and predicts SavE-HS89 as the potential candidate for the solar vapour adsorption cooling systems. The preference selection index value of SavE-HS89 obtained is 0.81218.

Table 8
Case study: percentage of savings.

Cases	Latent heat (kJ/h)	Sensible heat(kJ/h)	Total heat (kJ/h)	Number of PCES unit	Total cost (€)	Savings (%)
Without fins	289	54	343	284	3296	—
Straight fin	405	76	481	202	2344	29%
Positive tapered fin	344	64	408	238	2762	16%
Negative tapered fin	539	101	640	152	1764	46%

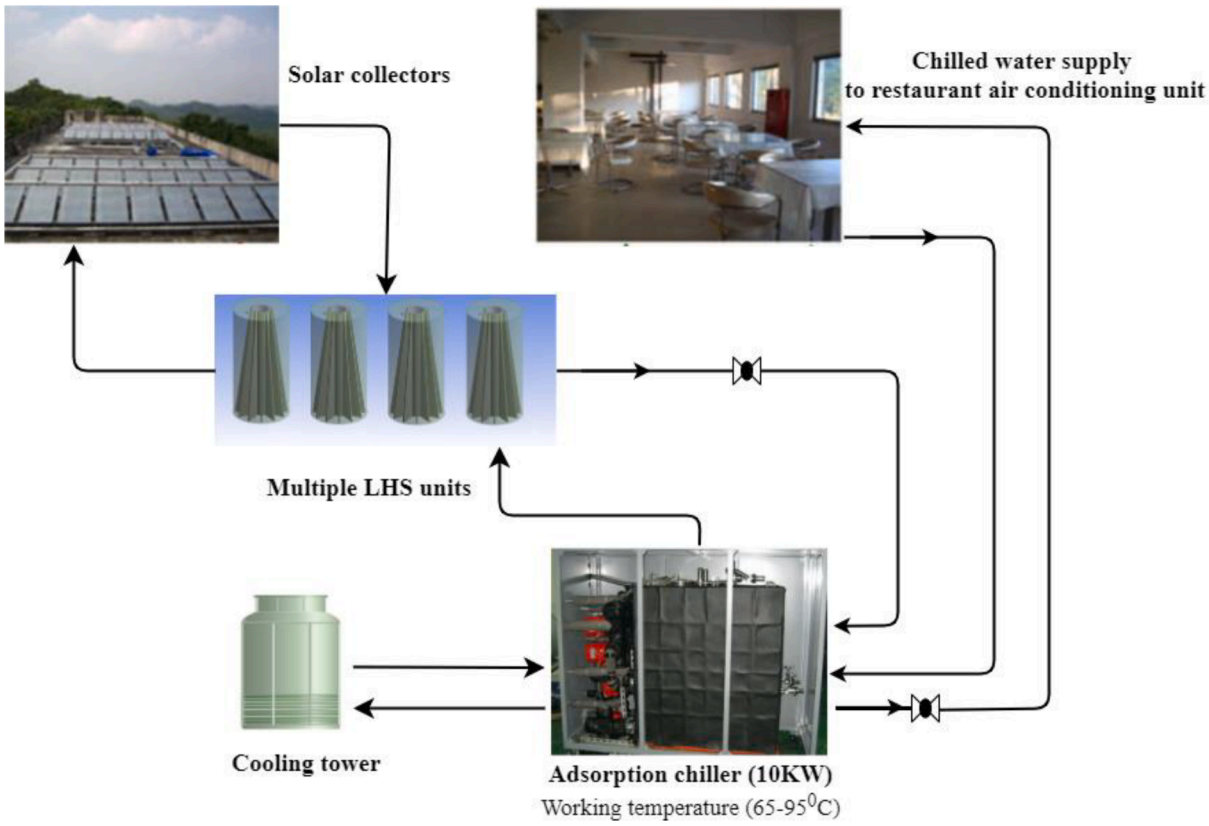

Fig. 15. Schematic diagram of Adsorption chiller integrated with PCES unit.

(b) A new design for PCES, effective for solar vapour adsorption cooling system is proposed, and three different fin shapes are tested. Negatively tapered fins are found to be more effective than conventional straight fins and positively tapered fins, with noticeable reductions in charging time of 13% and 36%, respectively.
(c) The value of Ø is significant and geometrical optimisation of negatively tapered fins shows Ø of 80% is considered to be the best choice for the design.
(d) Reynolds number of heat transfer fluid plays an important role during the melting of PCM. Reynolds number in the turbulent range can effectively reduce the melting time up to 45%.
(e) Analysis of designed PCES unit, integrated to an adsorption chiller of 10 kW capacity shows the importance of negatively tapered fins in SAC systems. Compared with the conventional finless design of the PCES unit, negatively tapered fin can reduce the number of PCES units and heat storage costs up to 25% and 46%, respectively.
(f) The above studies of PCES and selection of PCM are very helpful in designing the actual solar vapour adsorption cooling systems integrated with thermal energy storage.

CRediT authorship contribution statement

V. Krishna Raj: Conceptualization, Methodology, Software, Validation, Investigation, Writing – original draft. **V. Baiju:** Conceptualization, Writing – review & editing, Supervision, Project administration. **Faras P. Junaid:** Supervision, Validation, Project administration.

Declaration of Competing Interest

The authors declare that they have no known competing financial interest or personal relationship that could have appeared to influence the work reported in this paper.

References

[1] International Energy Agency (IEA), "The Future of Cooling Opportunities for Energy- Efficient Air Conditioning" International Energy Agency Website: www.iea.org, 2018, (2018).
[2] A.A. Sha, V. Baiju, Thermodynamic analysis and performance evaluation of activated carbon-ethanol two-bed solar adsorption cooling system, Int. J. Refrig. 123 (2021) 81–90, https://doi.org/10.1016/j.ijrefrig.2020.12.006.
[3] X.Q. Zhai, R.Z. Wang, A review for absorbtion and adsorbtion solar cooling systems in China, Renew. Sustain. Energy Rev. 13 (2009) 1523–1531, https://doi.org/10.1016/j.rser.2008.09.022.
[4] R.Z. Wang, Z.Z. Xia, L.W. Wang, Z.S. Lu, S.L. Li, T.X. Li, J.Y. Wu, S. He, Heat transfer design in adsorption refrigeration systems for efficient use of low-grade thermal energy, Energy 36 (2011) 5425–5439, https://doi.org/10.1016/j.energy.2011.07.008.
[5] I.I. El-Sharkawy, M. Hassan, B.B. Saha, S. Koyama, M.M. Nasr, Study on adsorption of methanol onto carbon based adsorbents, Int. J. Refrig. 32 (2009) 1579–1586, https://doi.org/10.1016/j.ijrefrig.2009.06.011.
[6] I.I. El-Sharkawy, B.B. Saha, S. Koyama, J. He, K.C. Ng, C. Yap, Experimental investigation on activated carbon-ethanol pair for solar powered adsorption cooling applications, Int. J. Refrig. 31 (2008) 1407–1413, https://doi.org/10.1016/j.ijrefrig.2008.03.012.
[7] A. El Fadar, Novel process for performance enhancement of a solar continuous adsorption cooling system, Energy 114 (2016) S1–S19, https://doi.org/10.1016/j.energy.2016.07.149.
[8] A.H. Poshtiri, A. Jafari, Reduction in auxiliary energy consumption in a solar adsorption cooling system by utilization of phase change materials, Journal of Solar Energy Engineering 138 (2017) 1–14, https://doi.org/10.1115/1.4033711.
[9] M. Sheikholeslami, S.A. Farshad, Z. Ebrahimpour, Z. Said, Recent progress on flat plate solar collectors and photovoltaic systems in the presence of nanofluid: a review, J. Clean. Prod. 293 (2021), 126119, https://doi.org/10.1016/j.jclepro.2021.126119.
[10] M. Sheikholeslami, M. Jafaryar, Z. Said, A.I. Alsabery, H. Babazadeh, A. Shafee, Modification for helical turbulator to augment heat transfer behavior of nanomaterial via numerical approach, Appl. Therm. Eng. 182 (2021), 115935, https://doi.org/10.1016/j.applthermaleng.2020.115935.
[11] M.C. Lin, C.C. Wang, M.S. Chen, C.A. Chang, Using AHP and TOPSIS approaches in customer-driven product design process, Comput. Ind. 59 (2008) 17–31, https://doi.org/10.1016/j.compind.2007.05.013.
[12] H. Xu, A. Romagnoli, J.Y. Sze, X. Py, Application of material assessment methodology in latent heat thermal energy storage for waste heat recovery, Appl. Energy. 187 (2017) 281–290, https://doi.org/10.1016/j.apenergy.2016.11.070.
[13] L. Socaciu, O. Giurgiu, D. Banyai, M. Simion, PCM selection using AHP method to maintain thermal comfort of the vehicle occupants, Energy Procedia 85 (2016) 489–497, https://doi.org/10.1016/j.egypro.2015.12.232.
[14] M. Rastogi, A. Chauhan, R. Vaish, A. Kishan, Selection and performance assessment of phase change materials for heating, ventilation and air-conditioning applications, Energy Convers. Manag. 89 (2015) 260–269, https://doi.org/10.1016/j.enconman.2014.09.077.
[15] Y. Wang, Y. Zhang, W. Yang, H. Ji, Selection of low-temperature phase-change materials for thermal energy storage based on the VIKOR method, Energy Technol. 3 (2015) 84–89, https://doi.org/10.1002/ente.201402098.
[16] K. Maniya, M.G. Bhatt, A selection of material using a novel type decision-making method: preference selection index method, Mater. Des. 31 (2010) 1785–1789, https://doi.org/10.1016/j.matdes.2009.11.020.
[17] R. Velraj, R.V. Seeniraj, B. Hafner, C. Faber, K. Schwarzer, Heat transfer enhancement in a latent heat storage system, Sol. Energy 65 (1999) 171–180, https://doi.org/10.1016/S0038-092X(98)00128-5.
[18] C. Nie, S. Deng, J. Liu, Numerical investigation of PCM in a thermal energy storage unit with fins: consecutive charging and discharging, J. Energy Storage 29 (2020), 101319, https://doi.org/10.1016/j.est.2020.101319.
[19] H. Babazadeh, M. Ramzan, N.D. Nam, M.R. Hajizadeh, Modeling for solidification of water within a triplex-tube tank using nanoparticles, J. Mol. Liq. 313 (2020), 113532, https://doi.org/10.1016/j.molliq.2020.113532.
[20] X. Zhang, M. Sheikholeslami, W.M. Yan, A. Shafee, F. Selimefendigil, H. Babazadeh, Energy storage analysis for discharging of nanoparticle enhanced phase change material within a triplex-tube thermal storage, J. Energy Storage 31 (2020), 101640, https://doi.org/10.1016/j.est.2020.101640.
[21] R.E. Murray, D. Groulx, Experimental study of the phase change and energy characteristics inside a cylindrical latent heat energy storage system: part 1 consecutive charging and discharging, Renew. Energy 62 (2014) 571–581, https://doi.org/10.1016/j.renene.2013.08.007.
[22] A.M. Abdulateef, S. Mat, J. Abdulateef, K. Sopian, A.A. Al-Abidi, Geometric and design parameters of fins employed for enhancing thermal energy storage systems: a review, Renew. Sustain. Energy Rev. 82 (2018) 1620–1635, https://doi.org/10.1016/j.rser.2017.07.009.
[23] D.S. Mehta, B. Vaghela, M.K. Rathod, J. Banerjee, Thermal performance augmentation in latent heat storage unit using spiral fin: an experimental analysis, J. Energy Storage. 31 (2020), 101776, https://doi.org/10.1016/j.est.2020.101776.
[24] M.S. Mahdi, A.F. Hasan, H.B. Mahood, A.N. Campbell, A.A. Khadom, A.M. em A. Karim, A.O. Sharif, Numerical study and experimental validation of the effects of orientation and configuration on melting in a latent heat thermal storage unit, J. Energy Storage. 23 (2019) 456–468, https://doi.org/10.1016/j.est.2019.04.013.
[25] M. Sheikholeslami, R. ul Haq, A. Shafee, Z. Li, Heat transfer behavior of nanoparticle enhanced PCM solidification through an enclosure with V shaped fins, Int. J. Heat Mass Transf. 130 (2019) 1322–1342, https://doi.org/10.1016/j.ijheatmasstransfer.2018.11.020.
[26] M. Majó, R. Sánchez, P. Barcelona, J. García, A.I. Fernández, C. Barreneche, Degradation of fatty acid phase-change materials (PCM): new approach for its characterization, Molecules 26 (2021) 1–11, https://doi.org/10.3390/molecules26040982.
[27] PlusICE Phase change material Product Ltd., PlusICE, Tech. DataSheet (2020). https://www.pcmproducts.net/files/PlusICE Range 2021-1.pdf. Accessed on 24th May 2021.
[28] Pluss Advanced Technologies, Pvt. Ltd., Tech. Data Sheet. (2018). https://www.pluss.co.in/upload/technical-datasheets/2019/Doc 308 TDS_HS89.pdf. Accessed on 24th May 2021.
[29] Rubitherm Technologies, RT-9HC, RT 90HC Tech. Datasheet Rmbh. (2020). https://doi.org/. Accessed on 24th May 2021.
[30] Rubitherm Technologies, Data Sheet Data Sheet, RT100 Tech. Datasheet Rmbh. (2020). https://www.rubitherm.eu/media/products/datasheets/Techdata_-RT100_EN_09102020.PDF, Accessed on 24th May 2021.
[31] Rubitherm Technologies, RT100HC, RT100 HC Tech. Datasheet Rmbh. (2020). https://www.rubitherm.eu/media/products/datasheets/Techdata_-RT100HC_EN_09102020.PDF., Accessed on 24th May 2021.
[32] P.B. Patel, J.D. Patel, K.D. Maniya, Application of PSI methods to select FDM process parameter for polylactic acid, Mater. Today Proc. 5 (2018) 4022–4028. https://doi.org/10.1016/j.matpr.2017.11.662.
[33] K. Yang, N. Zhu, C. Chang, D. Wang, S. Yang, S. Ma, A methodological concept for phase change material selection based on multi-criteria decision making (MCDM): a case study, Energy 165 (2018) 1085–1096, https://doi.org/10.1016/j.energy.2018.10.022.
[34] T. Mukhamet, S. Kobeyev, A. Nadeem, S.A. Memon, Ranking PCMs for building façade applications using multi-criteria decision-making tools combined with energy simulations, Energy 215 (2021), 119102, https://doi.org/10.1016/j.energy.2020.119102.
[35] M. Akgu, K. Kaygusuz, Experimental study on melting /solidification characteristics of a paraffin as PCM, 48 (2007) 669–678. https://doi.org/10.1016/j.enconman.2006.05.014.
[36] S. Tiwari, G.N. Tiwari, I.M. Al-Helal, Performance analysis of photovoltaic-thermal (PVT) mixed mode greenhouse solar dryer, Sol. Energy. 133 (2016) 421–428, https://doi.org/10.1016/j.solener.2016.04.033.
[37] W. Chang, C. Wang, C. Shieh, Design and performance of a solar-powered heating and cooling system using silica gel /water adsorption chiller, Appl. Therm. Eng. 29 (2009) 2100–2105, https://doi.org/10.1016/j.applthermaleng.2008.10.021.